VESSEL EXTRACTION USING CROSSING-ADAPTIVE MINIMAL PATH MODEL WITH ANISOTROPIC ENHANCEMENT AND CURVATURE CONSTRAINT

Li Liu[1,2] *Da Chen*[2,3] *Laurent D. Cohen*[2] *Huazhong Shu*[1] *Michel Pâques*[3]

[1] Laboratory of Image Science and Technology, the Key Laboratory of Computer Network and Information Integration, Southeast University,210096 Nanjing, China
[2]Université Paris Dauphine, PSL Research University, CNRS, UMR 7534, CEREMADE, 75016 Paris, France
[3]Centre Hospitalier National d'Ophtalmologie des Quinze-Vingts, Paris, France

ABSTRACT

In this work, we propose a new minimal path model with a dynamic Riemannian metric to overcome the shortcuts problem in vessel extraction. The invoked metric consists of a crossing-adaptive anisotropic radius-lifted tensor field and a front freezing indicator. It is able to reduce the anisotropy of the metric on the crossing points and steer the front evolution by freezing the points causing high curvature of a geodesic. We validate our model on the DRIVE and IOSTAR datasets, and the segmentation accuracy is 0.861 and 0.881, respectively. The proposed method can extract the centreline position and vessel width efficiently and accuracy.

***Index Terms*—** Geodesic, anisotropy enhancement, Riemannian metric, path feature, tubular structure segmentation

1. INTRODUCTION

Vessel extraction is a crucial step in computer-assisted therapy applications [1]. The minimal path method is a suitable and efficient tool for vessel structure delineation, in which vessels are modelled as minimal paths associated to metrics. However, it is prone to the shortcuts problem and an example is given in Fig. 1. A proper metric has essential importance in minimal path model, many improvements on which have been studied to address different situations in tubular structure segmentation.

The classic Eikonal PDE-based minimal path framework [2] proposes an isotropic Riemannian metric to measure the minimal path length, but it only delineates the vessel centerline. To further obtain the corresponding width of the vessel, the abstract radius variable is added to the image domain to construct the radius-lifted metric [3]. The anisotropic Riemannian metric taking into account the orientation information is also widely studied to solve the shortcuts problem by the orientation enhancement [4, 5]. Besides, the curvature information is utilized to obtain a smooth minimal path such as the sub-Riemannian metric [6] and an Finsler elastica metric with curvature penalization [7].

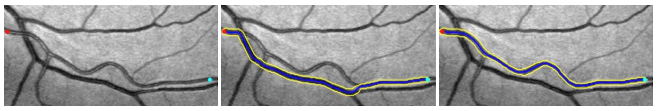

Fig. 1: An example of the shortcuts problem. **Column 1** A retinal image patch with prescribed points manually (red and cyan dots). **Column 2** and **3** Minimal paths (blue curve) obtained from [4] and the proposed method, respectively. Yellow curve represents the vessel boundary.

Let $\Omega \subset \mathbb{R}^2$ be a 2-dimensional image domain. The multi-scale space is defined as $\bar{\Omega} := \Omega \times [r_{\mathrm{l}}, r_{\mathrm{h}}]$, where $[r_{\mathrm{l}}, r_{\mathrm{h}}]$ is the radius space. We denote by $\mathcal{S}_d^+$ the set of symmetric positive definite matrices with size of $d \times d\,(d = 2, 3)$ and let $\mathrm{Lips}([0,1], \bar{\Omega})$ be the set of Lipchitz continuous curves $\gamma : [0,1] \to \bar{\Omega}$. A minimal path is a curve $\gamma \in \mathrm{Lips}([0,1], \bar{\Omega})$ minimizing the path length $\mathfrak{L}$ globally measured through a radius-lifted anisotropic Riemannian metric $\mathcal{M} : \bar{\Omega} \to S_3^+$

$$\mathfrak{L}(\gamma) = \int_0^1 \sqrt{\gamma'(t)^{\mathrm{T}} \mathcal{M}(\gamma(t)) \gamma'(t)}\, dt. \tag{1}$$

where the metric $\mathcal{M}$ can be expressed as

$$\mathcal{M}(\bar{\mathbf{x}}) = \begin{pmatrix} \mathcal{M}_{\mathrm{a}}(\bar{\mathbf{x}}) & \mathbf{0} \\ \mathbf{0} & \mathcal{P}_{\mathrm{s}}(\bar{\mathbf{x}}) \end{pmatrix}, \tag{2}$$

where $\bar{\mathbf{x}} = (\mathbf{x}, r) \in \bar{\Omega}$, $\mathcal{M}_{\mathrm{a}} : \bar{\Omega} \to S_2^+$ is a tensor field associated to the spatial anisotropy and $\mathcal{P}_{\mathrm{s}} : \bar{\Omega} \to \mathbb{R}^+$ is a scalar function. Once the metric is determined, the minimal curve length between the source point $\bar{\mathbf{s}}$ and any point $\bar{\mathbf{x}}$ can be characterized by the geodesic distance map as

$$\mathcal{U}_{\bar{\mathbf{s}}}(\bar{\mathbf{x}}) = \inf_{\gamma \in \mathrm{Lips}([0,1], \bar{\Omega})} \{\mathfrak{L}(\gamma); \gamma(0) = \bar{\mathbf{s}}, \gamma(1) = \bar{\mathbf{x}}\}. \tag{3}$$

It is the unique viscosity solution to the Eikonal PDE as

$$\|\nabla \mathcal{U}_{\bar{\mathbf{s}}}(\bar{\mathbf{x}})\|_{\mathcal{M}^{-1}(\bar{\mathbf{x}})} = 1, \forall \bar{\mathbf{x}} \in \Omega \backslash \{\bar{\mathbf{s}}\}, \tag{4}$$

with $\mathcal{U}_{\bar{\mathbf{s}}}(\bar{\mathbf{s}}) = 0$. A geodesic $\hat{\mathcal{C}}_{\bar{\mathbf{x}},\bar{\mathbf{s}}}$ linking $\bar{\mathbf{x}}$ to $\bar{\mathbf{s}}$ can be tracked by solving the gradient descent ordinary differential equation:

$$\hat{\mathcal{C}}'_{\bar{\mathbf{x}},\bar{\mathbf{s}}}(t) = -\frac{\mathcal{M}^{-1}(\hat{\mathcal{C}}_{\bar{\mathbf{x}},\bar{\mathbf{s}}}(t)) \nabla \mathcal{U}_{\bar{\mathbf{s}}}(\hat{\mathcal{C}}_{\bar{\mathbf{x}},\bar{\mathbf{s}}}(t))}{\|\mathcal{M}^{-1}(\hat{\mathcal{C}}_{\bar{\mathbf{x}},\bar{\mathbf{s}}}(t)) \nabla \mathcal{U}_{\bar{\mathbf{s}}}(\hat{\mathcal{C}}_{\bar{\mathbf{x}},\bar{\mathbf{s}}}(t))\|}, \tag{5}$$

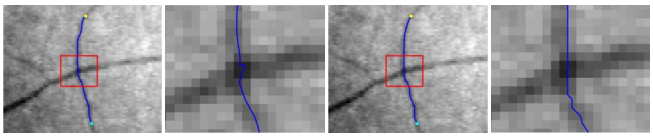

Fig. 2: Reducing the anisotropy of metric on crossing point. **Column 1** and **3** Minimal paths (blue curve) detected by [4] and the proposed crossing-adaptive metric, respectively. **Column 2** and **4** The region within the red rectangle. (Yellow and cyan points are prescribed manually.)

with $\hat{\mathcal{C}}_{\bar{\mathbf{x}},\bar{\mathbf{s}}}(0) = \bar{\mathbf{x}}$. The final geodesic $\mathcal{C}_{\bar{\mathbf{s}},\bar{\mathbf{x}}} \in \mathrm{Lips}([0,1],\bar{\Omega})$ can be obtained by reversing and reparameterizing $\hat{\mathcal{C}}_{\bar{\mathbf{x}},\bar{\mathbf{s}}}$.

In this work, we have proposed a dynamic anisotropic Riemannian metric depending on the geometric information and path feature in radius-lifted space, where the associated minimal paths favour to pass the vessel smooth.

2. THE NEW ANISOTROPIC GEODESIC METRIC WITH NONLOCAL INFORMATION

The main goal in this section is to establish a new Riemannian metric $\mathcal{M}_{\mathrm{d}}$ expressed by

$$\mathcal{M}_{\mathrm{d}}(\bar{\mathbf{x}}) = \mathcal{M}(\bar{\mathbf{x}})\delta(\bar{\mathbf{x}}), \forall(\bar{\mathbf{x}}) \in \bar{\Omega}. \tag{6}$$

It consists of two ingredients: the crossing-adaptive anisotropic radius-lifted tensor field $\mathcal{M} : \bar{\Omega} \to S_2^+$ and the front freezing indicator $\delta : \bar{\Omega} \to \{1, \infty\}$, which will be described in Sections 2.1 and 2.2.

2.1. Crossing-Adaptive Tensor Field

We suppose that the intensities inside the tubular structures are lower than background. The crossing-adaptive tensor field $\mathcal{M}$ can be constructed by blocks as Eq. (2), which is based on an optimal direction $\mathbf{v}_1(\bar{\mathbf{x}})$ at each point $\bar{\mathbf{x}}$ and the corresponding eigenvalue λ_2 characterizing the appearance feature. The eigenvalues λ_i $(i = 1, 2, \cdots, d)$ extracted from the optimally oriented flux filter [8] are the values of oriented flux along the corresponding eigenvectors $\mathbf{v}_i$, which are computed by $\lambda_i(\bar{\mathbf{x}}) = \mathbf{v}_i^T(\bar{\mathbf{x}})\,\mathbf{F}(\bar{\mathbf{x}})\mathbf{v}_i(\bar{\mathbf{x}})$. The optimal scale map $\eta : \Omega \to [r_{\mathrm{l}}, r_{\mathrm{h}}]$ is defined to obtain the optimal direction and vesselness map by:

$$\eta(\mathbf{x}) = \underset{r\in[r_{\mathrm{l}},r_{\mathrm{h}}]}{\arg\max} \{\lambda_2(\mathbf{x}, r)\}\,. \tag{7}$$

We define the vesselness map $\zeta : \Omega \to \mathbb{R}_0^+$ and the tubular feature vector $\mathfrak{p} : \Omega \to \mathbb{R}^2$ at the optimal scale η:

$$\zeta(\mathbf{x}) = \max\{\lambda_2(\mathbf{x}, \eta(\mathbf{x})),\, 0\}\,, \mathfrak{p}(\mathbf{x}) = \mathbf{v}_1(\mathbf{x}, \eta(\mathbf{x})). \tag{8}$$

The shortcuts problem often occurs at a crossing point due to the vector $\mathfrak{p}(\cdot)$ usually indicates the orientation of the stronger vessel at this crossing point. So the speed computed from the anisotropic metric is slower along the weak vessel than that along the strong one. Therefore, the shortcuts problem usually happens as shown in Column 2 of Fig. 1. Or the obtained geodesic is not smoothed within the crossing region as shown in Column 1 and 2 of Fig. 2. To solve these problems, the anisotropy of the metric on crossing points are reduced by utilizing the crossing-adaptive structure tensors as described in work [9]. The spatial anisotropy tensor filed $\mathcal{M}_{\mathrm{a}}$ and scalar function $\mathcal{P}_{\mathrm{s}}$ of $\mathcal{M}$ are shown as

$$\mathcal{M}_{\mathrm{a}}(\bar{\mathbf{x}}) = \exp(-\alpha\lambda_2(\bar{\mathbf{x}}))\mathcal{T}_{\mathrm{s}}(\bar{\mathbf{x}}), \mathcal{P}_{\mathrm{s}}(\bar{\mathbf{x}}) = \beta\exp(-\alpha\lambda_2(\bar{\mathbf{x}})). \tag{9}$$

where parameters $\alpha,\ \beta \in \mathbb{R}^+$ control the regularization of the spatial dimensions and radius dimension. The tensor field $\mathcal{T}_{\mathrm{s}} : \bar{\Omega} \to S_2^+$ is computed via a Gaussian kernel G_p with standard derivative p and the the identity matrix $\mathrm{I_d}$ as

$$\mathcal{T}_{\mathrm{s}}(\mathbf{x}, \cdot) = \Big((G_p * \mathcal{T})(\mathbf{x})/(G_p * \hbar)(\mathbf{x}) + \epsilon\,\mathrm{I_d}\Big)^{-1}, \tag{10}$$

where $\mathcal{T}(\mathbf{x}) = \hbar(\mathbf{x})\mathfrak{p}(\mathbf{x})\mathfrak{p}^T(\mathbf{x})$. The parameter $\epsilon \in \mathbb{R}^+$ is a sufficiently small constant to avoid the singularity, and $\hbar : \Omega \to \mathbb{R}_0^+$ is a weighted function to reduce the influence from the regions outside the vessel structures. We set $\hbar \cong \zeta$ (Eq. (8)) in this work. If $\mathbf{x}$ is a vessel point and the vector $\mathfrak{p}$ changes slowly, then the eigenvector of the tensor $(G_p * \mathcal{T})(\mathbf{x})$, which corresponds to the largest eigenvalue, will approximate to the feature vector $\mathfrak{p}(\mathbf{x})$. For the vessel points nearby a crossing structure, the feature vectors potentially vary fast leading to that the tensors $(G_p * \mathcal{T})(\mathbf{x})$ are nearly isotropic. So the obtained geodesic is smooth within the crossing region as shown in Column 3 and 4 of Fig. 2.

2.2. Front-Freezing Indicator

The front-freezing indicator is computed based on the path feature derived from the curvature of the local geodesic through two extra points $\bar{\mathbf{m}}$, $\bar{\mathbf{z}}$ located on it like the method in [10]. The local geodesic can be computed through solving the gradient descent ODE (Eq. (5)) on the obtained geodesic distance map. Let $|\mathcal{C}|$ denote the geodesic length. Backtracking from $\bar{\mathbf{x}}$ stops when $|\mathcal{C}_{\bar{\mathbf{x}},\bar{\mathbf{z}}}| = \Gamma$, where Γ is a constant and $\bar{\mathbf{z}}$ is the back-tracked truncated point. The point $\bar{\mathbf{m}}$ is another extra point defined as the middle point along the local geodesic. The curvature $\mathcal{K}$ is measured by the angle between two vectors from the local geodesic as in [11] as:

$$\mathcal{K}(\bar{\mathbf{x}}) = \langle(\bar{\mathbf{m}} - \bar{\mathbf{z}}), (\bar{\mathbf{x}} - \bar{\mathbf{m}})\rangle/(\parallel \bar{\mathbf{m}} - \bar{\mathbf{z}} \parallel \parallel \bar{\mathbf{x}} - \bar{\mathbf{m}} \parallel), \tag{11}$$

where $\langle\cdot,\cdot\rangle$ denotes scalar product, $||\cdot||$ represents the norm of the vector. The range of $\mathcal{K}$ is $[1, -1]$.

The indicator is constructed to determine the curvature range of the tubular structure as

$$\delta(\bar{\mathbf{x}}) = \begin{cases} 1 & \mathcal{K}(\bar{\mathbf{x}}) > \mathcal{K}_0 \\ +\infty & \text{otherwise} \end{cases}, \tag{12}$$

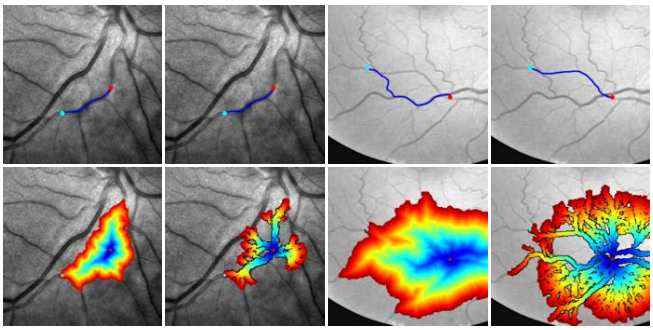

Fig. 3: **Raw 1** Retinal image patches with minimal path (blue curve) and prescribed points (red and cyan dots). **Raw 2** Geodesic distances superimposed on the original images. **Column 1** and **3** are computed from [4]. **Column 2** and **4** are obtained by the proposed model (Frozen points are denoted as black dots.).

where $\mathcal{K}_0$ is a given threshold. If the value of $\mathcal{K}$ for the current point is bigger than the given threshold, the wavefront is propagated as usual, otherwise the point is frozen. The indicator takes into account the curvature constraint in order to seek geodesics without sharp turnings. Such an indicator is motivated by the fact that the retina blood vessels usually appear as linear structures with low curvatures. As an example, we show the frozen points violating the criterion as black points as shown in Column 2 and 4 of Fig. 3.

Algorithm 1 Fast Marching Method

Output: Minimal action map $\mathcal{U}_{\mathrm{s}}$.
Initialization: Set $\forall \bar{\mathbf{x}} = (\mathbf{x}, r) \in \bar{\Omega} \setminus \{\bar{\mathbf{s}}\}$, set $\mathcal{U}_{\bar{\mathbf{s}}}(\bar{\mathbf{x}}) \leftarrow \infty$, $\mathcal{L}(\bar{\mathbf{x}}) \leftarrow Far$; $\mathcal{U}_{\bar{\mathbf{s}}}(\bar{\mathbf{s}}) \leftarrow 0$, $\mathcal{L}(\bar{\mathbf{s}}) \leftarrow Trial$; $\mathcal{F}(\mathbf{x}) \leftarrow 0$.

```
while stopping criterion is not reached do
    Find x̄_m minimizing U_s̄ and set L(x̄_m) ← Accepted;
    if F(x_m) = 0 then
        Compute curvature K via Eq. (11);
        if K ≤ K_0 then
            Set U_s̄(x̄_m) ← ∞ and F(x_m) ← 1;
        else
            for all ȳ ∈ H(x̄_m) and L(ȳ) ≠ Accepted do
                Set L(ȳ) ← Trial and compute U_s̄(ȳ);
            end for
        end if
    else
        Set U_s̄(x̄_m) ← ∞;
    end if
end while
```

3. FAST MARCHING IMPLEMENTATION

In the course of fast marching front propagation, all the grid points are labeled as three classes: Far, $Trial$ and $Accepted$. The geodesic distance is estimated by solving the Hopf-Lax operator defined in [12]. The stencil $\mathcal{N}(\bar{\mathbf{x}})$ determines the neighbourhood for each point $\bar{\mathbf{x}}$, and its inverse neighbourhood can be described as $\mathcal{H}(\bar{\mathbf{x}}) := \{\bar{\mathbf{y}} \in \mathbb{Z}^3; \bar{\mathbf{x}} \in \mathcal{N}(\bar{\mathbf{y}})\}$. The procedure for the fast marching method is described in Algorithm. 1.

The proposed Riemannian tensor field $\mathcal{M}_{\mathrm{d}}$ is updated during the geodesic distance computation which is actually carried out by computing the front-freezing indicator in the front advancing procedure to determine whether the front points should be frozen or not. In implementation, once a point $(\mathbf{x}, r)$ is frozen, all the points at position $\mathbf{x}$ with different radius scale belonging to $[r_{\mathrm{l}}, r_{\mathrm{h}}]$ will be frozen and tagged as $Accepted$. This scheme is helpful to save calculation consuming. It is achieved by defining a flag map $\mathcal{F} : \Omega \to \{0, 1\}$, where $\mathcal{F}(\mathbf{x}) = 1$ denotes that the point at position $\mathbf{x}$ is frozen. During fast marching fronts propagation, once the point $(\mathbf{x}, r)$ with minimal geodesic on the front is chosen, the value of $\mathcal{F}(\mathbf{x})$ can be checked. For better visualization, we consider a new distance map $\mathcal{U}^*_{\bar{\mathbf{s}}}$ obtained by minimzing $\mathcal{U}_{\bar{\mathbf{s}}}$ over the last dimension

$$\mathcal{U}^*_{\bar{\mathbf{s}}}(\mathbf{x}) = \min_{r \in [r_{\mathrm{l}}, r_{\mathrm{h}}]} \{\mathcal{U}_{\bar{\mathbf{s}}}(\mathbf{x}, r)\}. \tag{13}$$

Examples for $\mathcal{U}^*_{\bar{\mathbf{s}}}$ are shown in Fig. 3.

4. EXPERIMENTAL RESULTS AND DISCUSSION

In this section, we evaluated our proposed model on 40 patches from the DRIVE[11] and 40 patches from IOSTAR[13] datasets. We consider $\Gamma = 8$ and $\mathcal{K}_0 = 0.9$ in the experiment. The parameter $\epsilon = 0.05$ is used to determine the anisotropic property of the structure tensor. Besides, $\alpha = 5$ and $\beta = 0.5$. The measurement is defined as:$\mathcal{R} = \#\|\mathcal{S} \cap \mathcal{G}\| / \#\|\mathcal{S}\|$, where $\mathcal{R} \in [0, 1]$ and $\#\|\cdot\|$ denotes the number of pixels within the set. Let $\mathcal{S}$ represents the segment result and $\mathcal{G}$ denotes the ground truth. $\mathcal{R} = 1$ means that the segmented result is exactly same with the ground truth.

We compare our proposed crossing-adaptive anisotropic radius-lifted tensor field $\mathcal{M}$ (caArR), the dynamic Riemannian metric $\mathcal{M}_{\mathrm{d}}$ (dArR) with the anisotropic radius-lifted Riemannian metric (ArR)[4]. Those methods detect the vessel region with centerlines and the boundaries. The result is shown in Table. 1. We also compare our method with the progressive minimal path model with dynamic speed proposed in [10], which only detects the vessel centerlines. The centerlines from the ground truth is dilated by a disk whose radius are 2 pixels, and the result is regarded as $\mathcal{G}$ in the measurement $\mathcal{R}$. The segmentation accuracy is 0.832 and 0.803, respectively.

Dataset	ArR	caArR	dArR
DRIVE	0.365	0.580	0.861
IOSTAR	0.790	0.815	0.881

Table 1: Quantitative comparison results on retinal images.

We compare the caArR metric with the classic ArR metric on retinal image patches, which are illustrated in Fig. 4. The

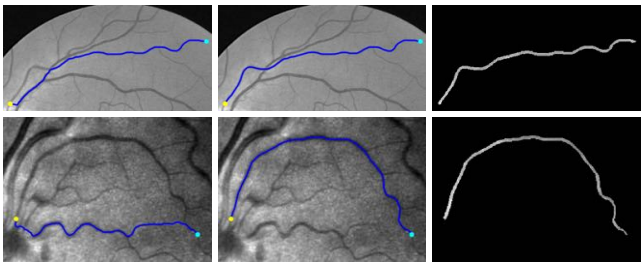

Fig. 4: Comparison results on retinal images. **Column 1**and **2** Minimal paths (blue curve) detected by [4] and the proposed crossing-adaptive metric, respectively. **Column 3** Vessel with thickness. Cyan and yellow dote are prescribed manually.

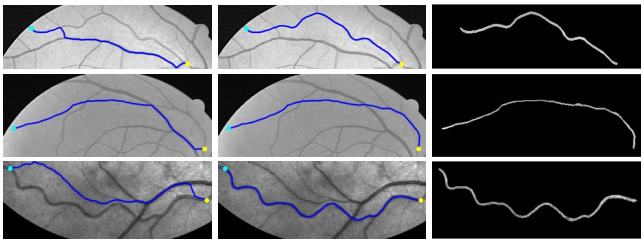

Fig. 5: Comparison results on retinal images. **Column 1**and **2** Minimal paths (blue curve) detected by [4] and the proposed model, respectively. **Column 3** Vessel with thickness. Cyan and yellow dote are predefined manually.

comparison of the dArR with ArR metric is shown in Fig. 5. We observe that the classic ArR metric suffered from shortcut problem in some situations. Our method is able to handle the hard situation by reducing the anisotropy in the crossing section and take into account the curvature feature. The centerline positions and boundaries can be tracked for the vessel between the two given points manually by the proposed interactive method.

5. CONCLUSION

In this paper, we have proposed a new minimal path model with a dynamic Riemannian metric for tubular structure segmentation by integrating the local geometric feature and nonlocal path feature. We construct the dynamic Riemannian metric during the fast marching front propagation. The quantitative and qualitative results demonstrate that our method indeed solves the shortcuts problem in some situations and detects the desired vessel region from complex background.

6. REFERENCES

[1] C. Kirbas and F. Quek, "A review of vessel extraction techniques and algorithms," *ACM Computing Surveys*, vol. 36, no. 2, pp. 81–121, 2004.

[2] L.D. Cohen and R. Kimmel, "Global minimum for active contour models: A minimal path approach," *IJCV*, vol. 24, no. 1, pp. 57–78, 1997.

[3] H. Li and A. Yezzi, "Vessels as 4-d curves: Global minimal 4-d paths to extract 3-d tubular surfaces and centerlines," *TMI*, vol. 26, no. 9, pp. 1213–1223, 2007.

[4] F. Benmansour et al., "Tubular structure segmentation based on minimal path method and anisotropic enhancement," *IJCV*, vol. 92, no. 2, pp. 192–210, 2011.

[5] S. Bougleux et al., "Anisotropic geodesics for perceptual grouping and domain meshing," in *ECCV*. Springer, 2008, pp. 129–142.

[6] E.J. Bekkers et al., "A pde approach to data-driven sub-riemannian geodesics in se (2)," *SIAM*, vol. 8, no. 4, pp. 2740–2770, 2015.

[7] D. Chen et al., "Global minimum for a finsler elastica minimal path approach," *IJCV*, vol. 122, no. 3, pp. 458–483, 2017.

[8] M. Law and A.C. Chung, "Three dimensional curvilinear structure detection using optimally oriented flux," in *ECCV*. Springer, 2008, pp. 368–382.

[9] M. Law et al., "Gradient competition anisotropy for centerline extraction and segmentation of spinal cords," in *IPMI*. Springer, 2013, pp. 49–61.

[10] W. Liao et al., "Progressive minimal path method for segmentation of 2d and 3d line structures," *PAMI*, vol. 40, no. 3, pp. 696–709, 2018.

[11] A Qureshi et al., "A bayesian framework for the local configuration of retinal junctions," in *CVPR*, 2014, pp. 3105–3110.

[12] J. Mirebeau, "Anisotropic fast-marching on cartesian grids using lattice basis reduction," *SIAM*, vol. 52, no. 4, pp. 1573–1599, 2014.

[13] J. Zhang et al., "Robust retinal vessel segmentation via locally adaptive derivative frames in orientation scores," *TMI*, vol. 35, no. 12, pp. 2631–2644, 2016.